J Neurophysiol 95: 1194–1206, 2006;
doi:10.1152/jn.00935.2005.

Cortico-Cerebellar Coherence During a Precision Grip Task in the Monkey

Demetris S. Soteropoulos[1,2] and Stuart N. Baker[1]

[1]*University of Newcastle, Sir James Spence Institute, Royal Victoria Infirmary, Newcastle upon Tyne; and* [2]*Department of Anatomy, University of Cambridge, Cambridge, United Kingdom*

Submitted 7 September 2005; accepted in final form 7 November 2005

Soteropoulos, Demetris S. and Stuart N. Baker. Cortico-cerebellar coherence during a precision grip task in the monkey. *J Neurophysiol* 95: 1194–1206, 2006; doi:10.1152/jn.00935.2005. We studied the synchronization of single units in macaque deep cerebellar nuclei (DCN) with local field potentials (LFPs) in primary motor cortex (M1) bilaterally during performance of a precision grip task. Analysis was restricted to periods of steady holding, during which M1 oscillations are known to be strongest. Significant coherence between DCN units and M1 LFP oscillations bilaterally was seen at ~10–40 Hz (contralateral M1: 25/87 units; ipsilateral: 9/87 units). Averaged coherence between DCN units and contralateral M1 LFP showed a prominent ~17-Hz coherence peak and an average phase of approximately $-\pi/2$ radians, implying that the DCN units fired around the time of maximal depolarization of M1 cells. The lack of a time delay between DCN and M1 activity suggests that the cerebellum and cortex may form a pair of phase coupled oscillators. Although coherence values were low (mean peak coherence, 0.018), we used a computational model to show that this probably resulted from the nonlinearity of spike generating mechanisms within the DCN. DCN unit discharge and DCN LFPs also showed significant coherence at ~10–40 Hz, with similarly low magnitude (mean peak coherence, 0.012). The average coherence phase was –2.5 radians for the 6- to 14-Hz range and −1.1 radians for the 17- to 41-Hz range, suggesting different frequency-specific underlying mechanisms. Finally, 4/40 pairs of simultaneously recorded DCN units showed a significant cross-correlation peak, and 16/40 pairs showed significant unit-unit coherence. The extensive oscillatory synchronization observed between cerebellum and motor cortex may have functional importance in sensorimotor processing.

INTRODUCTION

Oscillations are ubiquitous in neural tissue, but there is still ongoing debate about their functional importance. In the visual system, oscillations may be involved in binding neurons responding to the same stimulus into a functional ensemble (Engel et al. 1990; Gray et al. 1989, 1990). A similar role has been proposed for olfactory systems (Stopfer et al. 1997). However, in the motor system, it has been more difficult to assign a plausible function.

Oscillations can occur in primary motor cortices (M1), as assessed by global markers of neural activity such as local field potentials (Baker et al. 1997; Murthy and Fetz 1996a; Sanes and Donoghue 1993), electro-encephalograms (Pfurtscheller and Neuper 1992; Pfurtscheller et al. 1993), and magneto-encephalograms (Conway et al. 1995; Kilner et al. 1999; Salenius et al. 1997). These oscillations can also be seen at the neuronal level: pairs of M1 neurons can show oscillatory cross-correlation peaks (Baker et al. 2001; Murthy and Fetz 1996b) and single cells (including pyramidal tract neurons [PTNs]) can be phase locked to oscillatory cortical ocal field potentials (LFPs) (Baker et al. 2003; Murthy and Fetz 1996b). Oscillations at ~15–30 Hz occur during rest or steady contraction and are abolished during active movements. They may be involved in attentional and preparatory processes for the forthcoming movements (MacKay 1997; Singer 1999). Cortical oscillatory activity affects spinal motoneurons, producing coherence at ~15–30 Hz between M1 recordings and contralateral EMG, probably through corticospinal pathways (Baker et al. 2003). Corticomuscular coherence is also only seen during steady contractions (Baker et al. 1997; Conway et al. 1995; Kilner et al. 1999). Such coherence with the periphery suggests that cortical oscillations may have a subtle role in peripheral calibration and probing of muscles (MacKay 1997).

Oscillations in the 10- to 40-Hz range showing a similar modulation with movement can be seen in several other cortical regions such as primary somatosensory area (Murthy and Fetz 1992; Nicolelis et al. 1995), parietal cortex (MacKay and Mendonca 1995), premotor cortex (Lebedev and Wise 2000), and supplementary motor area (Lee 2004). Task-modulated coherence between areas has also been shown (Murthy and Fetz 1996a; Roelfsema et al. 1997). This may support a role in a form of motor binding (Jackson et al. 2003; Konig and Engel 1995; MacKay 1997).

Task-modulated oscillations also occur in cerebellar cortex in the 10- to 25-Hz range (Courtemanche et al. 2002; O'Connor et al. 2002; Pellerin and Lamarre 1997). As in motor cortex, oscillations in the cerebellar granule cell layer disappear during movements (Hartmann and Bower 1998; Pellerin and Lamarre 1997), and in primates are more prominent during nonmovement attentive task epochs (Pellerin and Lamarre 1997). In the rat, oscillations are coherent between cerebellar cortex (Crus II) and S1 (O'Connor et al. 2002). Purkinje cells are phase locked to such oscillations (Courtemanche et al. 2002), presumably transmitting them to the deep cerebellar nuclei (DCN), although the impact on DCN units has not been fully studied. Recently Aumann and Fetz (2004) showed that cerebellar interpositus cells have significant coherence with muscle activity (EMG), which may implicate the DCN in the network responsible for corticomuscular coherence. The DCNs have strong projections to M1 through thalamus (Asanuma et al. 1983; Aumann et al. 1994; Chan-Palay 1977; Hoover and Strick 1999; Kelly and Strick 2003), and oscillatory activity in M1 and thalamic relay neurons can be triggered by activity in cerebello-fugal fibers (Timofeev and Steriade 1997). Marsden et al. (2000) showed thalamo-cortical and thalamo-muscular coherence at 8–27 Hz in tremor patients with no cerebellar

Address for reprint requests and other correspondence: S. N. Baker, Sir James Spence Inst., Royal Victoria Infirmary, Newcastle upon Tyne NE1 4LP, UK (E-mail: stuart. baker@ ncl.ac.uk).

The costs of publication of this article were defrayed in part by the payment of page charges. The article must therefore be hereby marked "*advertisement*" in accordance with 18 U.S.C. Section 1734 solely to indicate this fact.

deficits, while this was not present in cases with cerebellar pathology.

In this report, we show that single units in the DCN (mainly nucleus interpositus) are phase locked to M1 LFPs at ~15–22 Hz during periods of steady muscle contraction. Although low, the coherence magnitudes are similar to those of M1 PTNs to M1 LFPs previously reported. As a population, DCN units will therefore transmit an oscillatory signal to M1 through thalamus. The phase of the M1-DCN coherence indicates near zero-phase coupling of the spike activity in each area. Given their distance apart, and the lack of the phase lags that would be expected from conduction delays, we propose that M1 and cerebellum behave as a pair of reciprocally coupled oscillators. We also report that DCN units phase lock to local DCN oscillations, although oscillatory synchrony between pairs of neurons is very weak.

METHODS

The data presented here were taken from two female adult rhesus macaques (E and T 5.8 and 6 kgs, respectively; 4 yr 3 mo and 4 yr 8 mo, respectively), trained to perform a bimanual precision grip task.

Behavioral task

The behavioral task was a modified version of the precision grip task described in Baker et al. (2001). The animal was presented with two precision grip manipulanda: one for the left and one for the right hand. Access to the levers of these manipulanda was obstructed by two clear plastic flags. A trial of the task commenced when the monkey placed both hands on switches located directly in front of the flags (see Fig. 1*A* for task timing). Some time after switch closure (0.45, 0.75, or 1.05 s), a cue was given indicating which movement should now be made. This cue consisted of a 6-Hz vibration of the flag, lasting for 1 s. Either the left flag alone, the right flag alone, or both together could vibrate, indicating respectively that left, right, or bimanual performance was required. Flag vibration was accompanied by flashing LEDs on the appropriate manipulandum, which also acted as cues. After the cue was an instructed delay period of 0.7, 1, or 1.3 s, during which the flags were stationary, and the animal was not permitted to remove its hands from the switches. At the end of this period, both flags moved down, permitting access to the manipulandum. The animal was required to move the correct hand or hands to grasp the two levers of the manipulandum between finger and thumb in a precision grip. Both levers had to be moved more than a criterion distance and held in this position for 1 s, before being released to obtain a food reward. Torque motors opposed these movements with forces that were proportional to lever displacement and hence simulated the action of springs. A force of 0.15 N was required for initial lever movement; after this, the force increased by 0.03 N/mm of lever travel. Performance on the task was cued to the animal by auditory tones indicating switch closure, cue delivery, precision grip squeeze, hold period termination, and reward delivery. Incorrect movements, or premature release of the switches, resulted in a failure tone and termination of that trial. The trial type (left, right, or bimanual) was chosen at random.

Surgical preparation

The animals were implanted with a stainless steel headpiece to allow atraumatic head fixation (Lemon 1984). Recording chambers were placed to allow access to the deep cerebellar nuclei, centered at stereotaxic coordinates P8.5, L4, and to hand area of M1, centered at stereotaxic coordinates A13, L18. All surgical operations were performed using aseptic technique under deep general anesthesia (2–2.5% isoflurane in 50:50 O_2:N_2O) and were followed by a full course of antibiotic (coamoxyiclav 140/35, 1.75 mg/kg clavulanic acid, 7 mg/kg amoxycillin; Synulox, Pfizer) and analgesic (buprenorphine; Vetergesic, 10 μg/kg; Reckitt and Colman Products) treatment (see Wetmore and Baker 2004). All procedures were carried out under appropriate licenses from the UK Home Office.

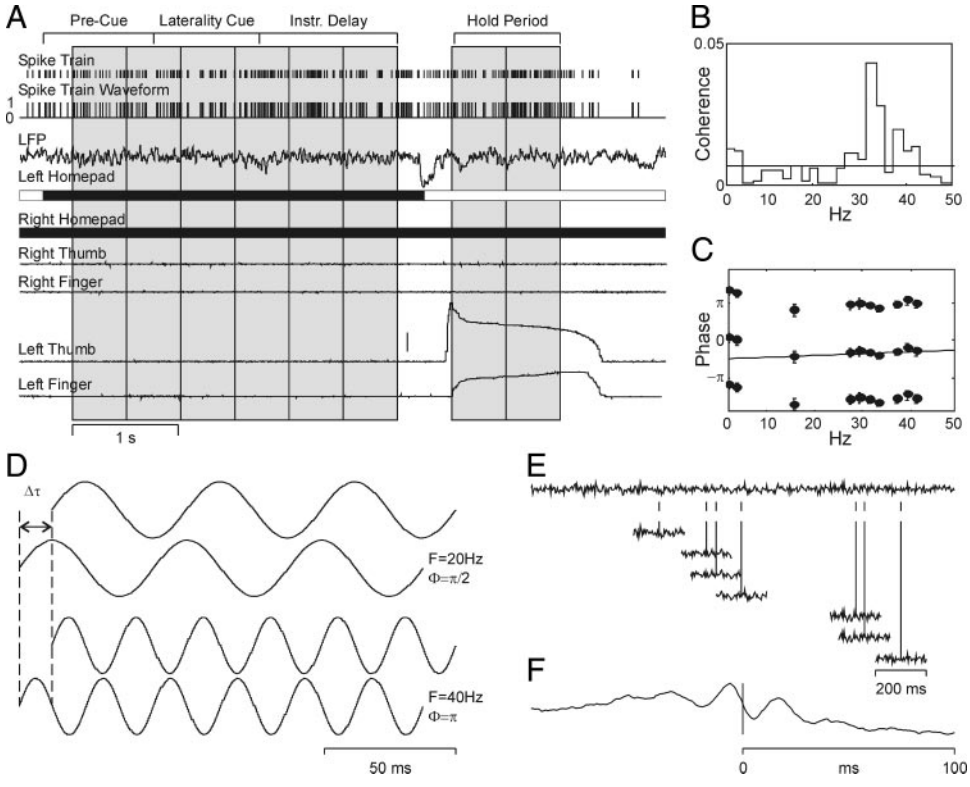

FIG. 1. Example of the methods used in this study. *A*: raw data from a single trial of the behavioral task, indicating neural spike firing, local field potentials (LFP), and measures of task performance. Gray boxes indicate data windows used for fast Fourier transform (FFT) analysis. *B*: example coherence spectrum. Horizontal line indicates significance level ($P < 0.05$). *C*: example phase spectrum. Solid line indicates a linear regression fitted to the phase values in the 6- to 41-Hz range (slope 0.025, not significantly different from 0). *D*: schematic illustration showing how a constant time delay results in a phase difference, which is linearly related to frequency. *E*: schematic showing the construction of a spike triggered average (STA). *F*: example STA of M1 LFP relative to a deep cerebellar nuclei (DCN) spike.

Placement of superior cerebellar peduncle stimulating electrodes

In monkey E, two stimulating electrodes (parylene insulated Tungsten, type LF01G, Microprobe) were chronically implanted into the superior cerebellar peduncles (SCPs) during the same surgery that implanted the cerebellar recording chamber.

To ensure accurate placement of these stimulating electrodes during surgery, a recording microelectrode was first inserted into the DCN (stereotaxic coordinates P8.5, L5). Localization of the DCN requires the ability to monitor the characteristic changes in extracellular spike activity as the electrode is lowered through cerebral cortex, cerebellar cortex, and into the DCN. However, this would be difficult under isoflurane anesthesia, which is known to depress neuronal activity (Berg-Johnsen and Langmoen 1987; Hentschke et al. 2005). Accordingly, for this part of the surgery, the inhaled isoflurane concentration was lowered progressively to 0.25%, while maintaining adequate anesthesia using ketamine (1 mg/kg). Pain from pressure points associated with fixation in the stereotaxic frame was blocked using subdermal bupivacaine (Marcain 0.5%, AstraZeneca) for the intraorbital margins, and EMLA cream (AstraZeneca) in the auditory meatus. Local anesthetic was applied before the animal was placed in the frame, several hours before the isoflurane anesthesia was lightened. Once the DCN electrode was correctly placed, the isoflurane levels were returned to normal (2–2.5%). Throughout the period when isoflurane anesthesia was lightened, the animal's heart rate remained steady and muscle tone was absent.

SCP electrodes were inserted, using a double angled approach. Craniotomies were drilled at arbitrary convenient locations on the skull. Their stereotaxic coordinates and those of the target (SCP at the decussation) were entered into a program that calculated the necessary angles. An SCP electrode was lowered through the craniotomy at these angles, while passing electrical stimuli (~300 μA, 1 Hz, 0.2-ms pulse width). The recording from the DCN electrode was monitored, and the SCP electrode was fixed at the point with the lowest threshold for an antidromic response (120 and 10 μA for left and right SCP electrodes, respectively). The coordinates of the final fixation points were A7, L0.7, H7.6 and A6 R0.7 H6.6 for the left and right electrodes, respectively. The DCN recording electrode was then removed.

Recordings

EMGs were recorded from seven forelimb muscles bilaterally through chronically implanted patch electrodes (Miller and Houk 1995). Cell activity from the DCN was recorded with an Eckhorn microdrive (Eckhorn and Thomas 1993), using glass insulated platinum tetrodes (Thomas Recording, Giessen, Germany). Six sharpened guide tubes (30 gauge) were inserted daily through the cortical dura mater at the desired coordinates, and penetrations were made through these to avoid electrode deviation. Entry into the cerebellum was determined from the characteristic sudden increase in activity on penetrating the tentorium. The electrodes encountered the layered patterns of activity characteristic of cerebellar cortex, followed by a region of electrical silence lasting around 1–3 mm. Entry into the DCN was indicated by the first cellular activity after this silence and was confirmed by observing the EMG and muscle twitch responses to trains of electrical stimuli delivered through one contact of each cerebellar tetrode (18 biphasic pulses at 300 Hz, maximum current 60 μA, 1-s interstimulus interval).

All four channels of each tetrode were amplified (gain 2000–10,000) and filtered (300 Hz to 10 kHz) to extract extracellular spiking activity. Spike waveform signals were continuously sampled at 25 kHz/channel. Waveform files were discriminated off-line into the occurrence times of single unit action potentials using custom written cluster-cutting software (Getspike; S. N. Baker; Spikelab; Dybal and Bhumbra 2003). Only units with consistent spike waveforms and no interspike intervals <1 ms were used for subsequent analysis.

The signal from one contact of each tetrode was also amplified (gain 2000) and filtered (3–100 Hz) to yield cerebellar local field potential. Cortical LFPs were recorded from both left and right M1 using chronically implanted electrodes. In monkey E, these consisted of Teflon-insulated 50-μm stainless steel wire (type 7907, A-M Systems). In monkey T, parylene-insulated tungsten microelectrodes were used (type WE30032.0A3, Microprobe). All LFP recordings used the stainless steel headpiece as the reference electrode. LFPs were continuously sampled at 500 Hz.

Coherence calculation

Coherence analysis was performed between single units and cortical and cerebellar LFPs and also between pairs of single units themselves. No coherence was calculated between cells and the LFP from the same electrode to avoid artifactual coherence arising from low frequency components of the spike waveform. In cases where there was more than one LFP recording from the same region, these were averaged to improve signal-to-noise ratio. An example of raw data from a single trial of the task is shown in Fig. 1*A*.

Single unit spike trains were converted to a waveform with the same sampling rate as the LFPs by counting spikes in 2-ms bins (Fig 1*A*, Spike train waveform). Fast Fourier transforms (FFTs) of 256 point data sections (Fig. 1*A*, gray boxes) were used to calculate coherence between unit spiking and LFP. Denoting the FFT of the *i*th segment of LFP by $X_i(f)$ and of the *i*th segment of unit data by $Y_i(f)$, the coherence was estimated as

$$Coh(f) = \frac{\left| \sum_{i=1}^{L} X_i^*(f) Y_i(f) \right|^2}{\sum_{i=1}^{L} X_i(f) X_i^*(f) \sum_{i=1}^{L} Y_i(f) Y_i^*(f)} \quad (1)$$

Where L is the number of data sections available for analysis, and * denotes complex conjugate. The use of 256 point segments provided a 1.95-Hz frequency resolution in the coherence spectra. An example coherence spectrum obtained in this way is shown in Fig. 1*B*.

Data were selected for cell to LFP coherence analysis to include only parts of the behavior with no active movements, because it is known that cortical oscillations are strongest at these times. Figure 1*A* shows a single trial of the task; the shaded boxes indicate the individual 256-point long data segments selected for analysis. These encompassed from the beginning of each trial until the go signal (end of instructed delay period) and the 1.024 s before the end hold period. All successful trials were used regardless of the laterality of task performance. Recordings were of insufficient length to allow separate analysis to be carried out for the different trial types (left, right, or bimanual).

A significance threshold level S was calculated for each cell to LFP pair, giving the coherence that should not be exceeded by chance $>95\%$ of the time if two signals are unrelated

$$S = 1 - 0.05^{\frac{1}{L-1}} \quad (2)$$

This estimate for the significance level was developed by Brillinger (1975) for stationary, Gaussian-distributed signals, although in previous work we have found it to be more widely applicable. For the present data set, we formed estimates of the coherence that would be expected by chance by shuffling the data segments X and Y, so that X_i was paired with $Y_j (j \neq i)$ in *Eq. 1*. The coherence was estimated from multiple different shuffled pairings, and the 95th percentile value was determined. This significance level for the coherence, determined by shuffling, agreed remarkably well with S determined from *Eq. 2* ($r = 0.9985$). We therefore used the level calculated from *Eq. 2* in the analysis presented in this paper, because this is computationally more straightforward and consistent with our previous work (Baker et al. 1997, 2003). In all coherence spectra, the significance level is shown by a horizontal line (Fig. 1*B*).

Coherence over the 6- to 41-Hz range was considered significant if it crossed the threshold S in four bins (a criterion chosen from the binomial distribution to give an overall significance level of $P < 0.05$). Only cell-LFP pairs that had >99 segments of data (each 256 points long) were included in the analysis. Where coherence was averaged across cells, significance levels were calculated as in Evans and Baker (2003).

If significant coherence in the 6- to 41-Hz range was seen, the coherence phase for the significant bins was calculated according to

$$\theta(f) = \arg\left(\sum_{i=1}^{L} X_i^*(f) Y_i(f)\right) \quad (3)$$

Phase was unwrapped if it lay close to $\pm\pi$ radians. For display purposes, each point was plotted three times, in the range -3π to $-\pi$, $-\pi$ to $+\pi$, and $+\pi$ to 3π, to assist visualization of phase-frequency relationships that cross arbitrary cycle boundaries (Fig. 1*C*). Error bars on phase plots were estimated as

$$\Delta\theta(f) = 1.96 \sqrt{\frac{1}{2L}\left(\frac{1}{Coh(f)} - 1\right)} \quad (4)$$

The range $(\theta - \Delta\theta)$ to $(\theta + \Delta\theta)$ represents ~95% confidence limits on the phase estimates (Rosenberg et al. 1989).

In situations where two signals are correlated with a fixed time delay, the phase difference between will be a linear function of frequency. This is shown schematically in Fig. 1*F*. The shown time delay, $\Delta t = 12.5$ ms, corresponds to a phase difference of $\pi/2$ at a frequency of 20 Hz, but to a phase difference of π at frequency of 40 Hz. To determine if there was evidence of fixed-delay coupling, a regression line was fitted to the phase-frequency relationship. If the slope was not significantly different from zero, the phase was assumed to be constant, and measured as the circular mean. If the slope was significantly different from zero ($P < 0.05$), the relationship between phase and frequency was characterized as a constant phase (value of regression line half-way across the frequency band of interest) plus a constant delay (slope of line).

For analysis of population data on phase of coherence, the circular mean phase ($\bar{\theta}$) and mean resultant length (R) were calculated as described in Fischer (1993)

$$Re^{i\bar{\theta}} = \frac{1}{N}\sum_{n=1}^{N} e^{i\theta_n} \quad (5)$$

where θ_n is the mean phase value of individual units. R has a value from 0 to 1 and indicates the degree of cancellation that would occur in a population average because of phase dispersion. $R = 0$ indicates complete cancellation and $R = 1$ indicates no cancellation.

Comparison of R between different phase distributions was performed by Monte Carlo (MC) sampling. The phase values from the two distributions were combined and randomly segregated to create two surrogate distributions. R was recalculated for each surrogate distribution. This was repeated 5,000 times. If the difference in R between the real phase distributions was greater than the difference in R between surrogates in 4,875 of the 5,000 MC runs, the phase distributions were considered to be significantly different ($P < 0.05$, 2-tailed).

In addition to the spectral analysis described above, spike triggered averages (STAs) of LFP were also compiled for illustrative purposes. Sections of the LFP recording were extracted time-aligned to the spikes (Fig. 1*E*) and averaged together (Fig. 1*F*). Such STAs reveal if the LFP has consistent modulations before or after the cell spike. Oscillatory correlations appear as damped oscillations in STA (Fig. 1*F*) but as narrow peaks in coherence spectra (Fig. 1*B*). Synchrony between pairs of single units in the time domain was assessed by the cross-correlation histogram (Perkel et al. 1967), which shows the occurrence of spikes from one cell as a function of time before and after spikes from a second cell.

Throughout, averaged values are given as mean ± SD.

Computational model

Because spike to LFP coherence is the coherence value between a cell's output and the LFP, simulations were run to obtain an indication of what the coherence between a cell's input and the LFP would need to be to obtain the coherence spectra reported here.

The model used was the same as in Baker et al. (2003), which should be consulted for more detail. Briefly, input to integrate-and-fire neurons was modeled as the sum of two independent sources of Gaussian random noise. One source was denoted as the LFP, whereas the second represented other uncorrelated synaptic inputs (noise). The LFP signal was attenuated in a frequency dependent manner, $X(f)$, where f here represents the frequency and X the attenuation. To keep the power at each frequency constant when the two signals were summed, the noise was attenuated by $1 - X(f)$. Given this, the coherence as a function of frequency of the model neuron's input with the LFP is by definition $X(f)$.

For each experimentally recorded cell, the input to the model cell was rescaled, so that the model neuron fired with the same mean rate as the real cell. The coherence between the model neuron's spike train and the LFP was compared with the experimental spectrum. $X(f)$ was adjusted in an iterative fashion until experimental and model coherence spectra were similar. If $C(f)$ denotes the experimental coherence spectrum, and $R_i(f)$ denotes the coherence spectrum obtained from iteration i of the model with parameters $X_i(f)$, we determined the fractional error in coherence as

$$\varepsilon_i(f) = \frac{R_i(f)}{C(f)} \quad (6)$$

Parameters were updated according to

$$X_{i+1} = \begin{cases} [k(\varepsilon_i - 1) + 1]X_i & \text{for } |R_i - C_i| > \Delta \\ X_i & \text{for } |R_i - C_i| \le \Delta \end{cases} \quad (7)$$

where the dependence of X, R, C, and ϵ on f has been suppressed for simplicity of notation. The value of the update sensitivity k was reduced successively from $k = 0.2$ to $k = 0.0005$. The allowable error in coherence Δ was set to 0.001. Typically, ~20 iterations were required for $R(f)$ at all frequencies to match $C(f)$ to within the allowable error Δ. Note that because the integrate-and-fire model used represents a nonlinear transformation from $X(f)$ to $R(f)$, we might expect changes in X at a single frequency will alter R at many frequencies. However, in practice this did not appear to be a significant problem: small changes in X altered R only at the frequencies changed. The iterative procedure described above therefore worked well.

At the end of this procedure, $X(f)$ provided an estimate of how large the coherence between LFP and synaptic inputs to the model neuron would need to be to reproduce the experimentally observed spike to LFP coherence spectrum.

Histology

At the end of the experiments, the monkeys were deeply anesthetized and perfused through the aorta with PBS (pH 7.2) followed by fixative. The cerebrum, cerebellum, and underlying brain stem were removed, processed, and stained with cresyl violet. Gliosis scars under microscopic examination were used to determine the likely target nucleus of the penetrations, although tracing individual microelectrode tracts was not possible because of the small size of the electrodes used (Mountcastle et al. 1991).

RESULTS

Thirty-seven single units were isolated from 30 penetrations in monkey T (15 right, 15 left cerebellum) and 50 single units from 30 penetrations in monkey E (2 right, 28 left cerebellum).

Cell identification

We encountered 24 SCP projection neurons and were able to record from 18 while the monkey performed the task. The units were identified by antidromic activation from the SCP electrode at a constant latency and through collision of an antidromic with a spontaneous spike (Lemon 1984).

An example collision test is shown in Fig. 2, *A–C*. For this cell, the collision interval was 0.4–0.6 ms. With an interval of 0.4 ms between the spike discriminator trigger output and the stimulus, collision occurred reliably (Fig. 2*A*). At an interval of 0.5 ms, it occurred in only two of seven sweeps (Fig. 2*B*), whereas no collision occurred at intervals 0.6 ms (Fig. 2*C*) and above. Swadlow et al. (1978) reported that axonal conduction velocity can vary depending on prior activity. The variability of the collision at the 0.5-ms interval was attributed to an activity-dependent change in conduction velocity.

The distribution of antidromic latencies of all projection neurons encountered is shown in Fig. 2*D*. The mean antidromic latency was 0.84 ± 0.24, and 12/24 latencies were <0.8 ms. The fastest antidromic latency was 0.6 ms. The straight line distance between the SCP stimulating electrodes and the DCN was determined from the stereotaxic coordinates of the SCP electrodes and the DCN recording electrode used during the implant surgery; this was 16.3 mm. An estimate of the fastest conduction velocity of the SCP axons is therefore 16.3/0.6 = 27 m/s. This will be an underestimate, because the axons follow a longer path than the straight line distance used in this calculation.

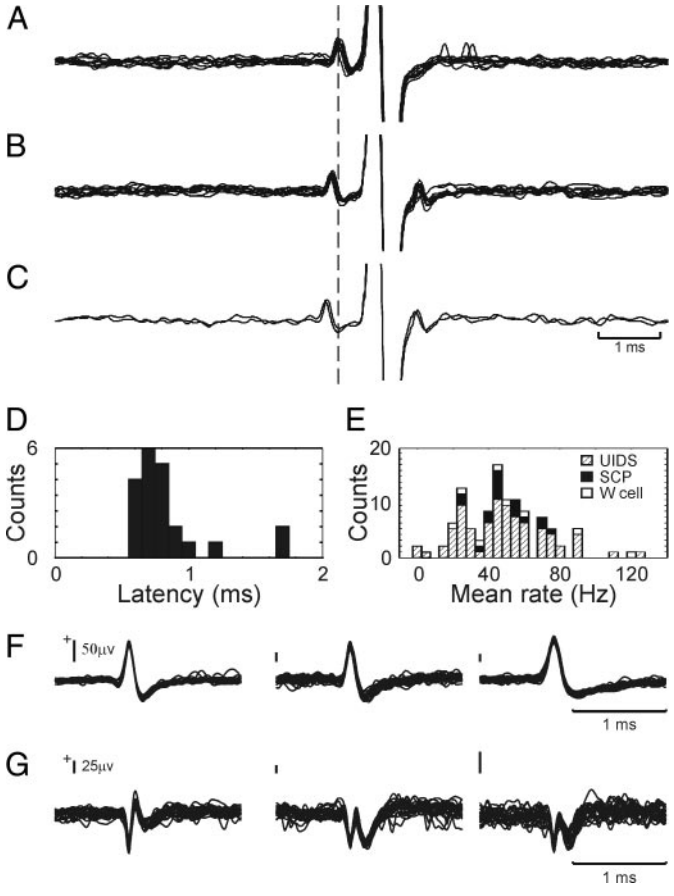

FIG. 2. Electrophysiological identification and characteristics of DCN neurons. *A–C*: collision test at 3 different intervals between spontaneous spike and antidromic spike elicited by superior cerebellar peduncles (SCP) stimulation (marked by stimulus artifact) *A*: 0.4-ms interval between spike trigger and stimulus. *B*: 0.5-ms interval. *C*: 0.6-ms interval. *D*: antidromic latency distribution of SCP units. *E*: mean firing rate of unidentified neurons (shaded), SCP neurons (black), and W cells (white). *F*: spike waveform of 3 SCP units. *G*: spike waveform of 3 UIDs with characteristic shapes. *F* and *G* show 25 spikes overlain.

The mean firing rate of all neurons recorded is shown in Fig. 2*E*; this was calculated using only parts of the recordings where the animal was performing the task. The black bars represent SCP-projecting neurons. The average firing rate of these cells was 51 ± 14 Hz compared with 50 ± 22 Hz for unidentified units.

SCP projection neurons had conventional biphasic action potentials, shown for three cells in Fig. 2*F*. The mean spike amplitude (peak-to-peak) was 141 ± 165 μV. We cannot draw any definitive conclusions about the identity of the other DCN neurons that did not respond antidromically to SCP stimulation. However, a small subset of these cells appeared different on the basis of the shape of their extracellular action potential, which was of a characteristic W shape (Fig. 2*G*). These cells were recorded just as the electrode entered the nucleus from the overlying white matter; electrical stimulation usually did not elicit muscle twitches in the vicinity of these cells, but did so when the electrode was advanced a few hundred microns. A total of 34 such cells were encountered in monkey E and held for long enough for the response to SCP stimulation to be tested. In no case could they be activated antidromically (maximum stimulus intensity tested, 300 μA). Seven such cells were recorded during task performance. Their average firing rate was 63 ± 63 Hz and mean spike amplitude was 41 ± 24 μV, neither of which were significantly different from the corresponding values for SCP projecting units (unpaired *t*-test, $P > 0.05$). Chan-Palay (1977) described a class of "boundary neurons" in monkey dentate nucleus. These cells are located at the edges of the nucleus and have dendrites that face toward the center of the nucleus but an outwardly projecting axon. The location of the cells with W-shaped action potentials fits with that of the boundary neurons, and it is possible that these are the same neural subtype.

Coherence between DCN single units and motor cortical LFP

Three example cells with significant coherence to M1 LFPs are shown in Fig. 3. Oscillations were often clearly visible in the spike triggered average of contralateral M1 LFPs (Fig. 3*A*), whereas in some cases, there were also oscillations visible for ipsilateral M1 (Fig. 3*D*).

For these cells, there was significant coherence in the 20- to 40-Hz range (Fig. 3*B*). The coherence phase was usually between 0 and $-\pi/2$ (Fig. 2*C*). By definition (*Eq. 3*), this indicates that the cell fired on average just after the negative peak of the LFP. In 5/25 cases, phase showed a significant linear relationship with frequency (Fig. 3*C3*). In two cases, the slope was negative, corresponding to the cell lagging the LFP (mean delay 10.2 ms, range 6–19.5 ms). In the remaining case, the slope was positive (implying LFP lagging the cell), with a delay of 17.6 ms.

Coherence at low-frequency bins (<6 Hz; Fig. 3*B2*) is likely to be caused by slow task-dependent comodulation in LFP and cell firing rate. The literature reports corticomuscular (Baker et al. 1997; Conway et al. 1995; Kilner et al. 1999; Salenius et al.

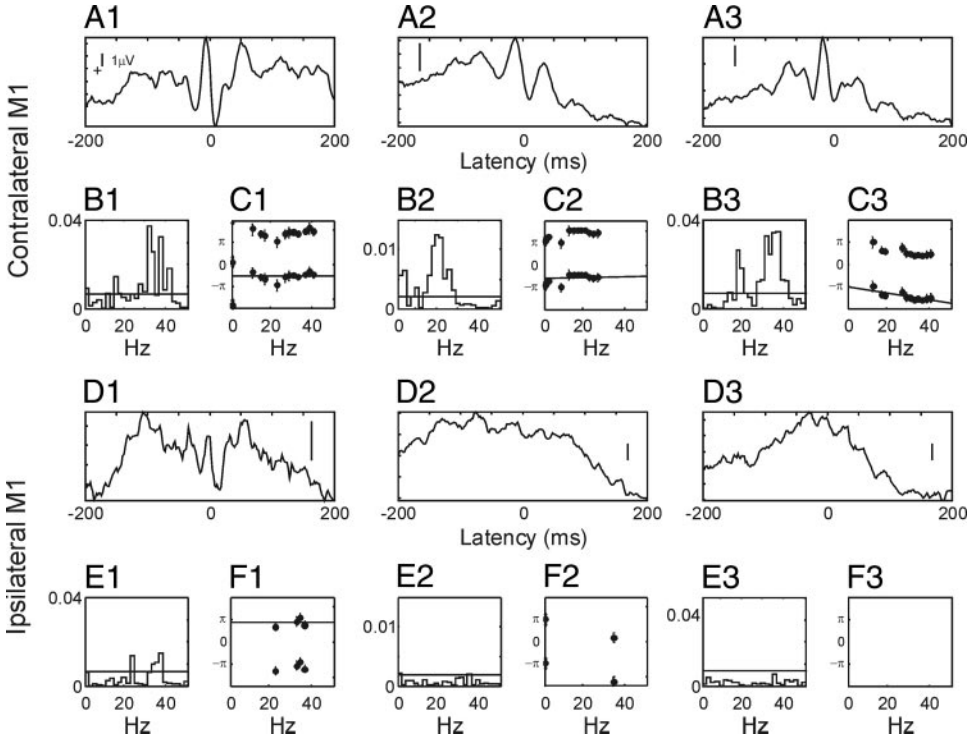

FIG. 3. Example correlation between 3 DCN cells and motor cortical LFP. *A*: spike triggered averages of LFP from contralateral M1. *B*: coherence of unit discharge with LFP from contralateral motor cortex. *C*: coherence phase. *D–F*: similar analysis as *A–C* for LFP from motor cortex ipsilateral to the DCN cells. Results from 3 neurons are shown, indicated by labels *1–3* throughout. Horizontal lines in *B* and *E* indicate calculated significance limit ($P < 0.05$). Lines in *C* and *F* indicate phase-frequency regression; that in *C3* had a slope significantly different from 0. Vertical calibration bars in *A* and *D* correspond to 1 μV.

1997) and corticocortical (Engel et al. 1990; Gray et al. 1989; Murthy and Fetz 1996a; Roelfsema et al. 1997; Sanes and Donoghue 1993) coherence at 10–50 Hz, and most cells showed effects below ~40 Hz. Further analysis therefore concentrated on the 6- to 41-Hz range. Only cells with significant coherence in 4 or more bins of the 17 bins in this range were considered further (this criterion being chosen from the binomial probability distribution to yield an overall significance level of $P < 0.05$).

In total, 25/87 cells from both monkeys (17 for monkey E: 6 projection neurons; 8 for monkey T) showed a significant coherence with contralateral M1, compared with 9 units that showed coherence with ipsilateral M1 (5 from monkey E: 2 projection neurons; 4 from monkey T). The mean coherence is shown in Fig. 4, *A* and *D*. This showed two distinct peaks for contralateral M1, at 15–22 and 32–39 Hz. Figure 4, *B* and *E*, shows the distribution of the peak coherence. The coherence values were small (all <0.05), but were not significantly different between ipsilateral and contralateral M1 (mean peak coherence: contralateral, 0.018 ± 0.015, ipsilateral 0.012 ± 0.063; $P > 0.05$, *t*-test).

Figure 4, *C* and *F*, shows the distribution of the mean coherence phase across the cell population showing significant coherence. For both ipsilateral and contralateral M1, the phase distributions were significantly different from uniform ($P < 0.01$, omnibus test; Fischer 1993). The dispersion of the phase estimates was measured using the mean resultant length measure R and was the same for both ipsilateral and contralateral LFP at 0.42. The circular mean phase θ for contralateral data were −1.34 radians (95% confidence limits, −1.17 to −1.5), and for ipsilateral data were 2.1 radians (0.52–3.7). Neither the peak coherence nor the coherence phase differed significantly between the different subcategories of cells (shown by different shading of the bars in Fig. 4); this may be because the small numbers of cells in each category prevented any differences from reaching significance. Only one W cell had significant coherence with contralateral M1.

Cell LFP coherence simulations

The coherence calculations performed here estimate the fraction of the variance in cell output spiking at a given frequency which is synchronous with the LFP. Although cell-LFP coherence values were low (<0.05), previous work has found similarly low values of coherence between M1 PTNs and LFPs (Baker et al. 2003). However, Baker et al. (2003) showed that a much higher proportion of the cells' inputs

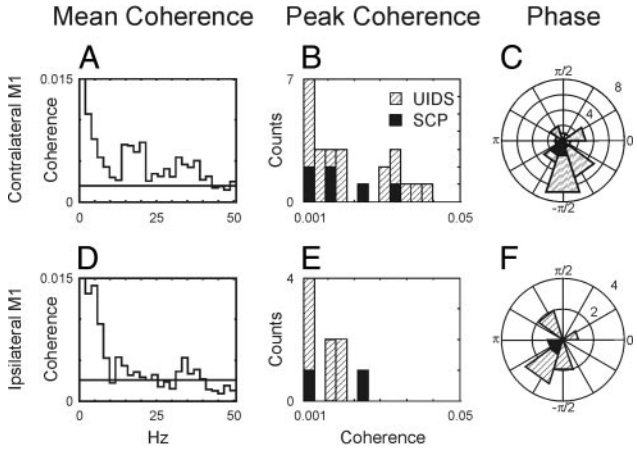

FIG. 4. Population analysis of DCN cell to cortical LFP coherence. *A*: mean coherence spectrum between 25 DCN units and LFP from contralateral M1. Horizontal line indicates calculated significance limit ($P < 0.05$). *B*: distribution of peak coherence between DCN units and contralateral M1 LFP over the frequency range of 6–41 Hz. *C*: distribution of coherence phase. *D–F*: similar analysis as *A–C*, but for coherence between DCN unit discharge and LFP from the ipsilateral M1. Black bars/slices in *B*, *C*, *E*, and *F* indicate antidromically identified SCP projection neurons; shaded bars are unidentified cells.

would need to be synchronous with the LFPs to obtain the experimentally observed coherence values; the difference was attributed to the nonlinearities introduced by the spiking threshold. We used a similar computational model as Baker et al. (2003) to determine how synchronous with M1 LFPs the inputs to the cerebellar units would need to be to obtain the small coherence values that we observed.

Figure 5 presents example results from this computational model. The dotted line in Fig. 5*A* plots the experimentally determined coherence between a DCN cell and the contralateral M1 LFP. This cell fired at an average rate of 24 Hz during the analysis period used. The solid line in Fig. 5*A* shows the coherence spectrum between the LFP and the output cell spiking of the computational model. Figure 5*B* shows a further example of experimental and simulated coherence spectra for a faster firing cell (80-Hz mean rate). The parameters of the model were adjusted to give a good match between experimental and simulated coherence spectra (see METHODS), and the closely overlapping curves of Fig. 5, *A* and *B*, confirm that this was achieved.

Figure 5, *C* and *D*, shows the value of the model parameter $X(f)$ for these two simulations, which represents the coherence between the LFP and the inputs to the model cell. Note the much higher scale on the ordinate compared with the cell-LFP coherence spectra. Figure 5*E* presents the mean coherence between DCN cells and the contralateral M1 LFP, and the average of $X(f)$ from simulations that individually matched each cell's experimental coherence spectrum and firing rate. At its ~17-Hz peak, the mean coherence was 0.0068, whereas the mean $X(f)$ was >10 times greater at 0.08. Similarly, peak values of $X(f)$ were much greater (mean, 0.14; Fig. 5*F*, shaded bars) than cell-LFP peak coherence values (mean, 0.018; Fig. 5*F*, black bars). The small coherences that we found experimentally therefore probably indicate that ~10% of the inputs to DCN neurons are synchronized with M1 LFP oscillations.

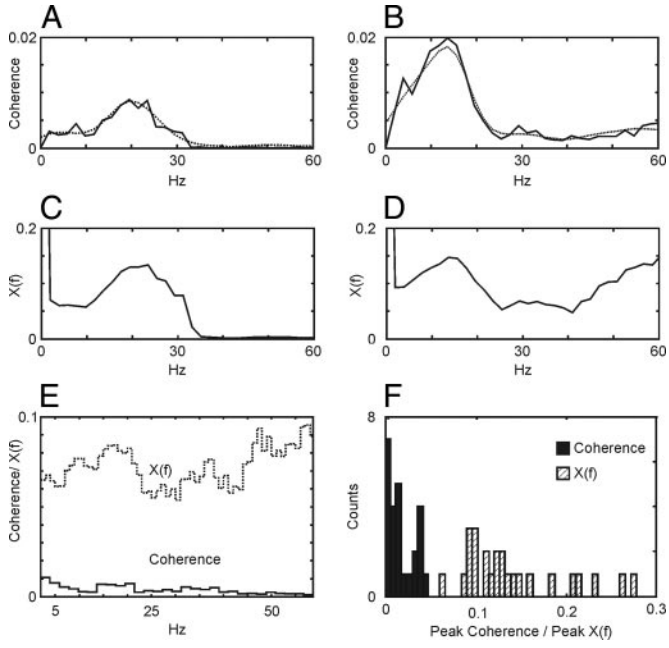

FIG. 5. Simulation results and comparison with real data. *A* and *B*: experimental (dotted line) and model (solid line) coherence spectra between cell discharge and contralateral M1 LFP for 2 different neurons. *C* and *D*: size of the model parameter $X(f)$ required to generate the model coherence spectra shown above in *A* and *B*. *E*: mean coherence spectrum (solid line) and $X(f)$ model parameter (dotted line), averaged over results from 25 neurons. *F*: distribution of peak coherence over the 6- to 41-Hz range for these cells (black bars) and of the peak $X(f)$ values (shaded bars).

Cell–cell interactions within cerebellar DCN

As sessions sometimes recorded multiple neurons simultaneously, it was possible to study interactions between DCN cells. In total, 63 pairs of neurons were available for analysis (49 in monkey E, 14 monkey T). Forty pairs had ≥10,000 spikes per cell simultaneously recorded with the other cell of the pair (35 monkey E, 5 monkey T).

Cross-correlograms (CrCs) were used to assess synchrony in the temporal domain. Significant short-term effects were found in only four pairs (Fig. 6, *A–D*, *left*). The latency of the cross-correlation peaks were all very close to zero (maximum latency, 0.4 ms), and all peaks were narrow (half-amplitude widths 1.2, 1.8, 3, and 2.6 ms for Fig. 6, *A–D*, respectively). The remaining CrCs showed no features above the noise level (example in Fig. 6*E*).

Coherence analysis was also performed between the spike trains of pairs of DCN cells, providing a frequency domain measure of correlation (Fig. 6, *A–E*, *middle*). Sixteen pairs showed significant coherence between 6 and 41 Hz (2 in monkey T, 14 in monkey E). The four pairs with peaks in CrCs all had significant coherence over a broad frequency band (Fig. 6, *A–D*, *middle*), indicative of nonoscillatory coupling. In the remaining 12 pairs, only a few bins rose above the significance level (example in Fig. 6*E*). The peak coherence was larger for the cells with CrC effects (Fig. 6*F*; mean 0.16 ± 0.076) compared with cells with flat CrCs (0.008 ± 0.0045). Figure 6, *G* and *H*, shows the mean coherence spectra for these two groups of cells. Most of the significant coherence for cells with no CrC peaks was <10 Hz.

Power spectral analysis was also performed on single unit spike trains, which is the analogue of an autocorrelogram in the time domain. The power spectra were normalized to have unit area, and the mean power spectra for each of the two monkeys is shown in Fig. 6*I*. There were no obvious peaks at frequencies >6 Hz.

The *right column* of Fig. 6, *A–E*, shows the coherence phase for the illustrated cells. For the four cells with CrC peaks (Fig. 6, *A–D*), phase was linearly related to frequency, indicating a constant time delay. The magnitude of this delay varied from 7 to 29 ms (mean, 12.5 ms), in contrast to the near zero-lag CrC peaks. This indicates that the coherence spectra were predominantly influenced by broader, secondary effects in the CrC, rather than the narrow central peak. Figure 6*J* shows a histogram of the mean phase in the 6- to 41-Hz range: values have been plotted twice with both positive and negative sign, because the sign arbitrarily depends on which cell is used as the reference event. Most phase values lay between 0 and $\pi/2$ (mean absolute phase, 1.1 radians; 95% confidence limits, 1.05–1.17 radians).

Cell to cerebellar LFP coherence

As a further measure of synchronization within the DCN, we determined the extent to which DCN neurons were phase locked to oscillations in the DCN LFP. Forty cells had significant coherence in the 6- to 41-Hz range. Figure 7, *A–C*, shows

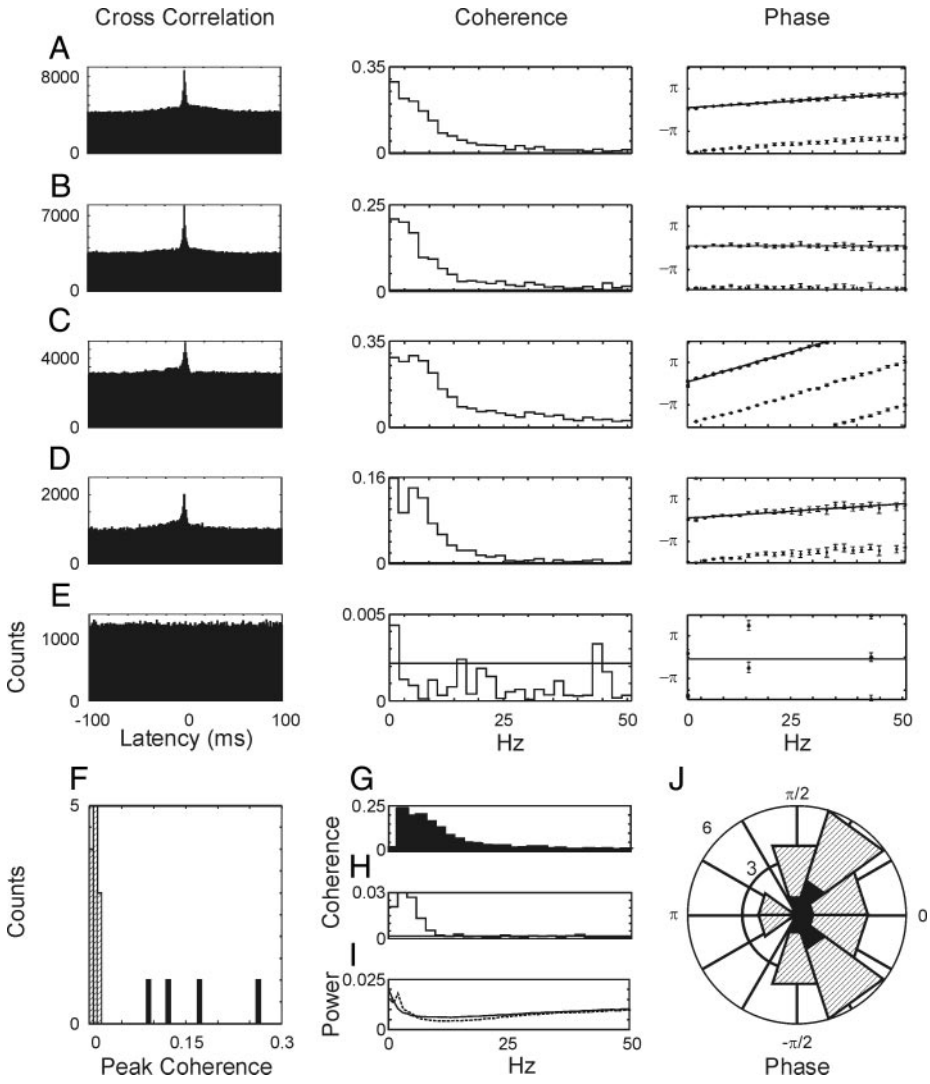

FIG. 6. Cell to cell correlation results in the temporal and frequency domains. *A–E*: cross correlograms (*left*), coherence spectra (*middle*), and phase spectra (*right*) for 4 pairs of DCN units with significant short-term correlation. *A–C* are from the same recording session. Horizontal lines on coherence plots show calculated significance limits ($P < 0.05$). Lines on phase spectra indicate phase-frequency regression fits, which had slopes significantly different from 0 for *A*, *C,* and *D*. *F*: distribution of peak coherence for 16 cell pairs with significant coherence in the 6- to 41-Hz range. *G*: mean coherence spectra of the 4 units with significant cross-correlation peaks shown in *A–D*. *H*: mean coherence spectra of remainder of units that had significant coherence. *I*: mean power spectra of unit spike trains for each monkey. Solid line is for units from monkey E, dotted line corresponds to monkey T. Power spectra are normalized to have unit area. *J*: distribution of coherence phase over the 6- to 41-Hz range. Phase values are plotted twice at both positive and negative signs. The 4 units with cross-correlation peaks (shown in *A–D*) have been plotted as black bars in *F–J*.

spike triggered averages of DCN LFP, coherence, and phase spectra for three examples.

Spike triggered averages often showed oscillatory features, although with very different periods (Fig. 7, *A–C*, *left*). The coherence spectra (Fig. 7, *A–C*, *middle*) showed distinct regions with significant coherence at ~10 and 20–40 Hz for the example cells shown. For these cells, phase was linearly related to frequency in the low-frequency band (Fig. 7*A*), whereas at the higher frequencies, the phase-frequency regression was flat (Fig. 7, *B* and *C*).

In the mean coherence spectrum, all bins were above the significance limit (Fig. 7*E*). However, there appeared to be separate peaks in coherence at ~10, 25, and 30 Hz. A histogram of the mean coherence phase across the 6- to 41-Hz band showed great variability across the cell population (Fig. 7*D*), as indicated by the low mean resultant length *R* of 0.19. The circular mean phase was −1.62 radians, but the 95% confidence limits were broad (−2.37 to 0.86).

The mean normalized power spectra of DCN LFPs showed substantial power over 6–41 Hz, with a decrease in power as frequency increased (Fig. 7*F*). In monkey E, there was a visible peak at ~10 Hz (Fig. 7*F*, solid line), whereas monkey T had visible peaks at ~25 and 41 Hz (Fig. 7*F*, dotted line).

Figure 7*E* suggests that the cell-DCN LFP coherence may be divided into two bands, with the division at ~15 Hz. Such a division is also suggested by the different behavior of coherence phase in these two regions (Fig. 7, *A–C*). A plot of the number of cells showing significant coherence in each frequency bin showed a clear dip at 17 Hz (Fig. 7*G*). Accordingly, we studied the effect of analyzing the distribution of the mean coherence phase separately for the two bands from 6 to 14 and 17 to 41 Hz (marked by gray and black shading, respectively, in Fig. 7*E*). Sixteen cells had significant coherence at 6–14 Hz (Fig. 7*H*). In 10/16 cases, the phase-frequency regression line had a slope significantly different from zero; the mean delay implied by this slope was 30 ms (range, −90 to 100 ms, positive delay corresponds to the cell leading the LFP). Given the small number of bins available for regression analysis, it is possible that some of the remaining six cells also showed a linear relationship, but with a slope too small to reach statistical significance. This mean delay may therefore be an overestimate. The circular mean phase was −2.5 radians (95% confidence limits, −3.2 to −1.9). The mean resultant length *R* was 0.34 but was not significantly different from *R* for 6–41 Hz ($P > 0.05$, MC sampling). Peak coherence values (mean, 0.0217 ± 0.028) for the 6- to 14-Hz band are shown in Fig. 7*I*.

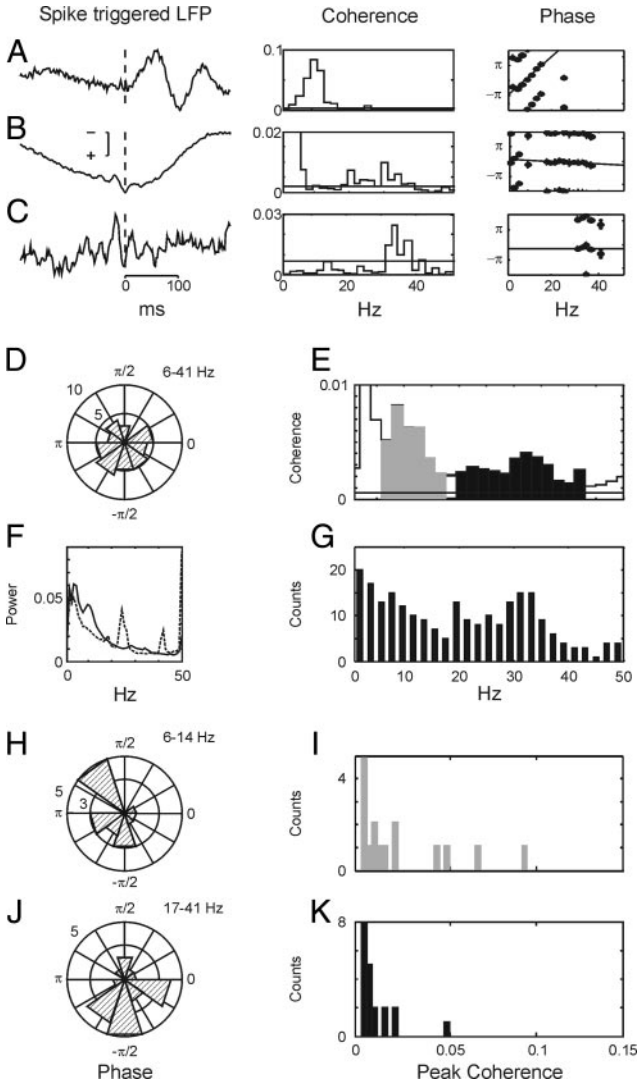

FIG. 7. DCN unit to DCN LFP coherence. *A–C*: spike triggered average (*left*), coherence spectra (*middle*), and phase plots (*right*) of 3 DCN units with DCN LFPs. Horizontal lines on coherence spectra show calculated significance limits ($P < 0.05$). Lines on phase spectra show phase-frequency regression fits; the slope in *A* was significantly different from 0. *D*: phase distribution of 40 cells with significant coherence between 6 and 41 Hz. *E*: mean coherence spectrum across this population. Area in gray corresponds to frequency range 6–14 Hz subsequently analyzed and shown in *H* and *I,* whereas area in black (17–41 Hz) is shown in *J* and *K*. *F*: mean power spectra of DCN LFPs for each monkey (solid line, monkey E; dotted line, monkey T). Power spectra were normalized to have unit area. *G*: number of cells showing coherence with DCN LFP at a particular frequency. *H*: phase distribution of 16 cells with significant coherence between 6 and 14 Hz. *I*: peak coherence for cells in *H*. *J*: phase distribution of 21 cells with significant coherence between 17 and 41 Hz. *K*: peak coherence for cells in *J*.

Twenty-one units had significant coherence with DCN LFPs in the 17- to 41-Hz band; only four of these had a significant delay (mean, –28 ms, range −55 to −4 ms). The phase distribution over this range of frequencies is shown in Fig. 7*J*. Although *R* was greater than that at 6–41 Hz (mean resultant length, $R = 0.4$), it was not significantly different ($P > 0.05$, MC sampling).

The circular mean phase was –1.1 radians (95% confidence limits, −1.35 to −0.8). Peak coherence values were similar to the low frequency band (mean, 0.0156 ± 0.036; Fig. 7*K*), although there were fewer extreme values >0.04.

Localization of recording sites

Given the deep location of the DCN, and the fine nature of our microelectrodes, reconstruction of individual recording tracks was not possible. However, histological examination of gliosis tracks in coronal sections suggested that, in both monkeys, the majority of the microelectrode penetrations to the DCN targeted the nucleus interpositus. In monkey T, there were also a few tracks toward medial dentate. Tracks heading for the fastigial nucleus were rarely seen. In addition, trains of stimuli (18 pulses, 300 Hz, ≤60 μA) were routinely given through the recording electrodes at the sites where cells had been recorded. While in many cases these evoked hand and forearm movements, they never produced stimulus evoked saccades. Because saccadic eye movements are often seen after stimulation in the fastigial nucleus (Noda et al. 1988), it is unlikely that any recordings were made from this nucleus.

We conclude that the majority of DCN cells in our database came from the nucleus interpositus, although a small fraction (probably <10%) may have come from the dentate.

DISCUSSION

Our results show that identified cerebellar output neurons carry an oscillatory signal, part of which is phase locked to oscillations in the activity of M1.

Neural subclasses

The results in all cases were similar for identified SCP projection neurons and unidentified cells. This is not surprising because most DCN units are likely to be projection neurons (Allen et al. 1977; Chan-Palay 1977; Tarnecki and Zurawska 1989): extracellular recordings will be biased against the less frequent and smaller local interneurons (Chan-Palay 1977). A clear subclass of unidentified cells did, however, emerge on the basis of extracellular action potential shape (W cells) and lack of antidromic activation. Based on their location at the edges of the nucleus, we suggest that these units may correspond to the boundary neurons reported by Chan-Palay (1977). Interestingly only one of seven of the recorded W cells had significant coherence with M1 LFP.

Pathways mediating cortico-cerebellar coherence

In this report, we showed significant oscillatory synchrony between DCN cells and contralateral M1. Such synchrony can only be produced by anatomical connections. Cerebello-cortical connectivity takes the form of a loop. Although most of our recordings probably came from the nucleus interpositus, this connectivity is similar for both the interpositus and dentate. On the descending side of this loop, the pons receives inputs from PTN collaterals as well as a separate system of cortico-pontine fibers (Kawamura and Chiba 1979; Ugolini and Kuypers 1986). It is known that the population discharge of PTNs can effectively transmit cortical oscillations (Baker et al. 2003), and it seems likely that other cortico-pontine fibers would also carry oscillations robustly. In vitro, pontine neurons show frequency dependent facilitation to paired pulses especially in the 20- to 50-Hz range (Mock et al. 1997); onward transmission of oscillatory input could therefore be especially effective over this frequency range. From the pons, oscillations could

reach the DCN directly through mossy fiber collaterals or after passage through the cerebellar cortex. Courtemanche et al. (2002) reported 13- to 25-Hz oscillations in Purkinje cell activity, once again implying that a selective enhancement of functionally relevant frequencies may occur. The ascending pathway from the DCN to M1 passes through potent excitatory connections to ventrolateral (VL) thalamus (Asanuma et al. 1983; Aumann et al. 1994; Chan-Palay 1977; Hoover and Strick 1999; Kelly and Strick 2003; Shinoda et al. 1985).

Importantly, both ascending and descending pathways introduce significant conduction delays. After electrical stimulation of the cerebral cortex, the earliest response in the DCN is seen ~5 ms later (Allen and Tsukahara 1974; Allen et al. 1977). Conversely, DCN stimulation facilitates single units in M1 with latencies of ~4 ms (Futami et al. 1986; Holdefer et al. 2000; Noda and Yamamoto 1984). Such conduction delays produce a characteristic linear phase-frequency relationship in the coherence phase spectra. The sign of the regression slope indicates which signal leads. In this paper, following from the definition of coherence phase in *Eq. 3*, a positive slope would indicate that the cortex leads the DCN, implying descending pathways are involved; conversely, a negative slope would indicate that the DCN leads the cortex, suggesting ascending pathway involvement.

Examination of the coherence spectra rarely revealed such a linear phase-frequency relationship for only 5/25 cells. Both positive and negative slopes were seen, implying either ascending or descending pathways could dominate for different cells. However, in most cells the phase was unrelated to frequency, and the phase across the cell population appeared clustered around $-\pi/2$ radians (Fig. 4). A similar result has been reported for the phase of PTNs with oscillations in M1 LFP (Baker et al. 2003). As described in that report, the $-\pi/2$ phase can be understood by considering the biophysics of extracellular recording. The extracellular field potential is proportional to the transmembrane current flowing through active synapses in the vicinity of the electrode tip. The transmembrane current is the derivative of intracellular potential (Hubbard et al. 1969). The operation of differentiation introduces a phase advance of $\pi/2$. Cells that show coherence with LFP at a phase of $-\pi/2$ are therefore firing synchronized at zero lag with postsynaptic potentials at the site of the LFP recording. Similar zero-lag synchrony has been shown in both visual and motor cortices between hemispheres, despite the known substantial conduction delays (Engel et al. 1990; Murthy and Fetz 1996a; Roelfsema et al. 1997). The zero-lag cortico-cerebellar synchrony observed here could not be produced by simple conduction in either ascending or descending pathways.

There are two possible ways in which zero-phase synchrony could be produced. First, DCN and M1 could receive common oscillatory input from a third source. One possible such source is the ascending pathways from the spinal cord, such as the spinocerebellar and spinothalamic tracts. In the lumbar spinal cord, there is evidence for coprojections to thalamus and cerebellum (Huber et al. 1994). The dorsal column nuclei project to both thalamus and cerebellum (Bermejo et al. 2003), although these projections are probably distinct and not collateralized (Massopust et al. 1985). However, to create zero-lag synchrony between M1 and the DCN, such input would need to arrive in the cortex and DCN with the same conduction delay. Because the cortex is dorsal to the cerebellum, spinal input is likely to be delayed in arriving at the cortex relative to the DCN. Common drive by an oscillatory source external to M1 and cerebellum therefore seems unlikely.

Alternatively, descending cortico-cerebellar pathways through the pons and ascending pathways through VL thalamus could both contribute to the observed coherence, causing M1 and the DCN to behave as a pair of reciprocally coupled oscillators. Such a circuit has been extensively studied using computational modeling (see Pauluis et al. 1999; Sturm and Konig 2001 for reviews). An important result of such work is that reciprocal coupling that is excitatory cannot on its own produce stable zero lag synchronization, because activity in each oscillator will tend to advance the firing of its counterpart (Ernst et al. 1995; Hansel et al. 1995; Van Vreeswijk et al. 1994).

Stable synchronization at zero-lag—even in the presence of a conduction delay—can be achieved in networks that include inhibition (Ernst et al. 1995; Gerstner 1996; Van Vreeswijk et al. 1994). If two neurons are reciprocally coupled by inhibition, when one fires, it will delay the firing of the other, and in turn receive inhibition later itself. Repeating this cycle leads to progressively tighter and tighter spike synchronization at zero phase lag (Ernst et al. 1995). Inhibition is a prominent component of cortico-cerebellar connectivity. Cortical stimulation produces a complex pattern of responses in the DCN consisting of multiple excitatory and inhibitory components (Allen and Tsukahara 1974; Allen et al. 1977; Shinoda et al. 1987). Thalamocortical neurons project to layers I, III, and VI of the motor cortex as well as layer V (Aumann et al. 1998; Noda and Yamamoto 1984; Strick and Sterling 1974), and thalamic stimulation produces reliable recruitment of fast-spiking interneurons (Beierlein and Connors 2002; Gibson et al. 1999). M1 spiking is depressed after DCN stimulation (Holdefer et al. 2000).

It is therefore plausible that zero-phase synchrony is achieved in this system through reciprocal coupling rather than exclusively by ascending or descending pathways. Interestingly, Riddle and Baker (2005) recently showed that cortico-muscular coherence is similarly likely to result from a complex interplay of ascending and descending pathways.

Although the above discussion has concentrated on the main ascending and descending pathways linking M1 and DCN, there exist several other indirect routes for signals to pass between these structures, and loops that could act to modify coherence phase. These include dentato-olivary, olivo-cerebellar, cortico-rubral, interposito- and dentato-rubral, and cortico-thalamic connections.

Some DCN units also showed coherence with ipsilateral M1, although this was generally smaller and without the prominent peaks seen with contralateral M1. The pathway mediating these effects is not clear at present. The pontine formation could also be responsible for mediating ipsilateral coherence because it projects to both sides of the cerebellum (Mihailoff 1983; Rosina et al. 1980). Alternatively, ascending connections could contribute, because there is a weak ipsilateral cerebello-thalamic projection (Aumann and Horne 1996; Chan-Palay 1977; Li and Tew 1966; Niimi et al. 1962). Finally, M1 shows interhemispheric synchrony (Murthy and Fetz 1996a), probably through transcallosal connections. This could produce the ipsilateral cerebello-cortical coherence as a consequence of the contralateral coherence seen.

Cerebellar encoding of oscillations

Previous reports have described oscillatory activity in the cerebellum and M1 separately; however, this is the first time that the synchronization between these oscillations has been studied. Cerebellar output neurons were coherent with M1 LFP oscillations over the 15- to 39-Hz range (Fig. 4*A*). Coherence values were low but similar to that seen between M1 PTNs and M1 LFPs (Baker et al. 2003). In both cases, the small coherence probably results from nonlinearities caused by neuron spiking. Using the same approach as Baker et al. (2003), we estimated that ~10% of the input to the DCN neurons was synchronous with M1 oscillations.

While the experimentally measured coherence spectra underestimate the extent of the synchrony between DCN inputs and M1 LFPs, they are an accurate measure of the encoding of M1 oscillations in DCN cell outputs. The very small values of coherence therefore indicate that a single DCN neuron represents this oscillatory signal poorly in its spike train. Even pairs of DCN cells failed to show oscillatory synchronization (Fig. 6): any synchrony seen was broadband in nature. However, Baker et al. (2003) showed that the summed population discharge of such weakly oscillatory cells could faithfully represent oscillations. There is considerable convergence from DCN to M1 (Shinoda et al. 1985), such that population averaging is likely to occur, improving the signal-to-noise ratio of oscillation transmission.

One additional condition must be met if an average population discharge is to represent oscillations effectively: the noise fraction of each cell's output discharge (i.e., that part uncorrelated with the oscillatory signal of interest) must be independent between the different cells (Baker et al. 2003; Shadlen and Newsome 1998). In this case, the noise will cancel when averaging multiple cell discharge, improving the population transmission of the oscillations. However, if the noise is correlated between cells, such cancellation will not occur, and the population spiking will be as poor a representation of the oscillations as the discharge of a single cell.

We found a low incidence and strength of synchrony between DCN cell pairs. The synchrony that was seen probably resulted from shared input, either from branched common input fibers (leading to the narrow cross-correlation peaks of Fig. 6, *A–D*) or through more indirect pathways. There are two reasons that this synchrony was so weak or absent. First, convergence is much more powerful than divergence in the corticonuclear projection, because ~800 Purkinje cells contact each DCN neuron, compared with each Purkinje cell contacting ~35 DCN neurons (Palkovits et al. 1977). This will reduce the number of inputs that are common between two cells. Second, a surprisingly large levels of common input is required to produce even a small amount of spike synchronization (Binder and Powers 2001; Halliday 2000). Whatever the cause, cross-correlation peaks were only rarely seen between the output spikes of DCN neuron pairs (Fig. 6). The requirement for low correlations between the noise component of each cell's discharge was therefore probably met, and DCN population spiking is likely to carry the M1 oscillatory signal with high fidelity.

One influential theory about cerebellar function is that the olivocerebellar system acts as an internal clock for motor output at ~10 Hz (Welsh and Llinas 1997; Welsh et al. 1995). This theory predicts that a coherent 10-Hz rhythm should be present in the DCN. There were indeed such oscillations in DCN LFPs (Fig. 7*F*), to which single unit activity could weakly phase lock (Fig. 7*E*). Keating and Thach (1997) have previously argued that DCN spike output contains no 10-Hz periodicity, based on the lack of 10-Hz peaks in single unit power spectra. Our single unit power spectra also showed no evidence for 10-Hz periodicity (Fig. 6*I*). However, the oscillatory signal is probably too weak to be revealed by single unit analysis and is visible only when analyzing a population measure such as the LFP.

Interestingly, although DCN-M1 coherence was significant over a wide range of frequencies, there was a pronounced dip in the mean coherence around 10 Hz (Fig. 4*A*). This is despite the prominent ~10-Hz oscillations in M1, which are routinely seen alongside those at higher frequencies (Baker et al. 2003; Pfurtscheller and Neuper 1992). A similar situation occurs for corticomuscular coherence: M1 oscillations around 25 Hz are coherent with those in contralateral EMG, but those at ~10 Hz have no significant coherence (Baker et al. 2003). The lack of significant M1-DCN coherence at ~10 Hz suggests that M1 is not the source of DCN oscillations at this frequency. There are a number of other possible sources, e.g., ascending input from the spinal cord, and our present data do not allow us to determine which might be most important. However, one of these possibilities remains the inferior olive, as suggested by the clock hypothesis of Welsh and Llinas (1997).

Functional implications of cerebro-cerebellar coherence

It is possible that the oscillatory synchrony that we have observed between cerebellum and cerebral cortex has no functional significance and is just an echo of cortical oscillations reverberating through the cerebello-cortical loops. However, there are other possibilities, which remain speculative at this stage.

One interesting potential function for these oscillations is as a sensorimotor sampling loop (MacKay 1997). This idea speculates that an oscillatory pulse is sent to the periphery to probe the muscular apparatus before or after movement. The afferent response from the periphery to this test pulse informs the brain about the status of the motor plant, which is essential information required for planning the next movement.

In support of this idea, oscillations are strongest during steady contractions before or after active movement (Baker et al. 1997; Kilner et al. 2000). Cortical oscillations do influence motoneurons, producing observable corticomuscular coherence (Baker et al. 1997; Conway et al. 1995). The properties of this corticomuscular coherence are inconsistent with generation by purely efferent pathways but suggest that afferents may also contribute (Riddle and Baker 2005). Finally, recent work indicates that afferent discharge does carry an oscillatory signal (S. N. Baker, M. Chiu, and E. E. Fetz, personal communication).

Critical to such an idea is the need to integrate both descending and ascending oscillatory activity. The interpositus (and the cerebellar cortex to which it connects) receives strong spinocerebellar feedback inputs from the periphery (Ito 1984; Oscarsson 1973; Somana and Walberg 1980), especially from muscle spindle afferents (Florence et al. 1989; Hummelsheim et al. 1985). It also receives cerebral inputs, including an

efference copy of descending corticospinal activity (Kawamura and Chiba 1979; Ugolini and Kuypers 1986). The intermediate cerebellum is therefore optimally placed to compare ascending and descending signals and to extract state-dependent information that this comparison might yield.

Whether or not the idea of a sensorimotor loop is correct, this study indicates that the cerebellum is intimately associated with the oscillatory network controlling movement, which also includes motor cortex, spinal cord, periphery, and afferent input. Any hypothesis for the functional role of these oscillations must explain why all of these components of the motor system synchronize their activity in this way.

ACKNOWLEDGMENTS

The authors thank S. Rhodes, D. Wetmore, and R. Pyper for assistance in collecting the experimental data.

GRANTS

This work was funded by the Wellcome Trust. D. Soteropoulos was also supported by the Leventis Foundation, the Wingate Foundation, the Cambridge Commonwealth Trust, and Christ's College, Cambridge.

REFERENCES

Allen GI, Gilbert PF, Marini R, Schultz W, and Yin TC. Integration of cerebral and peripheral inputs by interpositus neurons in monkey. *Exp Brain Res* 27: 81–99, 1977.

Allen GI and Tsukahara N. Cerebrocerebellar communication systems. *Physiol Rev* 54: 957–1006, 1974.

Asanuma C, Thach WT, and Jones EG. Distribution of cerebellar terminations and their relation to other afferent terminations in the ventral lateral thalamic region of the monkey. *Brain Res* 286: 237–265, 1983.

Aumann TD and Fetz EE. Oscillatory activity in forelimb muscles of behaving monkeys evoked by microstimulation in the cerebellar nuclei. *Neurosci Lett* 361: 106–110, 2004.

Aumann TD and Horne MK. Ramification and termination of single axons in the cerebellothalamic pathway of the rat. *J Comp Neurol* 376: 420–430, 1996.

Aumann TD, Ivanusic J, and Horne MK. Arborisation and termination of single motor thalamocortical axons in the rat. *J Comp Neurol* 396: 121–130, 1998.

Aumann TD, Rawson JA, Finkelstein DI, and Horne MK. Projections from the lateral and interposed cerebellar nuclei to the thalamus of the rat: a light and electron microscopic study using single and double anterograde labelling. *J Comp Neurol* 349: 165–181, 1994.

Baker SN, Olivier E, and Lemon RN. Coherent oscillations in monkey motor cortex and hand muscle EMG show task-dependent modulation. *J Physiol* 501: 225–241, 1997.

Baker SN, Pinches EM, and Lemon SN. Synchronization in monkey motor cortex during a precision grip task. II. Effect of oscillatory activity on corticospinal output. *J Neurophysiol* 89: 1941–1953, 2003.

Baker SN, Spinks R, Jackson A, and Lemon RN. Synchronization in monkey motor cortex during a precision grip task. I. Task-dependent modulation in single-unit synchrony. *J Neurophysiol* 85: 869–885, 2001.

Beierlein M and Connors BW. Short-term dynamics of thalamocortical and intracortical synapses onto layer 6 neurons in neocortex. *J Neurophysiol* 88: 1924–1932, 2002.

Berg-Johnsen J and Langmoen IA. Isoflurane hyperpolarizes neurones in rat and human cerebral cortex. *Acta Physiol Scand* 130: 679–685, 1987.

Bermejo PE, Jimenez CE, Torres CV, and Avendano C. Quantitative stereological evaluation of the gracile and cuneate nuclei and their projection neurons in the rat. *J Comp Neurol* 463: 419–433, 2003.

Binder MD and Powers RK. Relationship between simulated common synaptic input and discharge synchrony in cat spinal motoneurons. *J Neurophysiol* 86: 2266–2275, 2001.

Brillinger DR. *Time Series. Data Analysis and Theory.* New York: Holt, Rinehart and Winston, 1975.

Chan-Palay V. *Cerebellar Dentate Nucleus, Organisation, Cytology and Transmitters.* New York: Springer-Verlag, 1977.

Conway BA, Halliday DM, Farmer SF, Shahani U, Maas P, Weir AL, and Rosenberg JR. Synchronization between motor cortex and spinal motoneuronal pool during the performance of a maintained motor task in man. *J Physiol* 489: 917–924, 1995.

Courtemanche R, Pellen JP, and Lamore Y. Local field potential oscillations in primate cerebellar cortex: modulation during active and passive expectancy. *J Neurophysiol* 88: 771–782, 2002.

Dyball R and Bhumbra GS. Digital spike discrimination combining size and shape elements. *J Physiol* 547P: D9, 2003.

Eckhorn R and Thomas U. A new method for the insertion of multiple microprobes into neural and muscular tissue, including fiber electrodes, fine wires, needles and microsensors. *J Neurosci Methods* 49: 175–179, 1993.

Engel AK, Konig P, Gray CM, and Singer W. Stimulus-dependent neuronal oscillations in cat visual-cortex - intercolumnar interaction as determined by cross-correlation analysis. *Eur J Neurosci* 2: 588–606, 1990.

Ernst U, Pawelzik K, and Geisel T. Synchronization induced by temporal delays in pulse-coupled oscillators. *Phys Rev Lett* 74: 1570–1573, 1995.

Evans CM and Baker SN. Task-dependent intermanual coupling of 8-Hz discontinuities during slow finger movements. *Eur J Neurosci* 18: 453–456, 2003.

Fischer NI. *Statistical Analysis of Circular Data*. Cambridge, UK: Cambridge University Press, 1993.

Florence SL, Wall JT, and Kaas JH. Somatotopic organization of inputs from the hand to the spinal gray and cuneate nucleus of monkeys with observations on the cuneate nucleus of humans. *J Comp Neurol* 286: 48–70, 1989.

Futami T, Kano M, Sento S, and Shinoda Y. Synaptic organization of the cerebello-thalamo-cerebral pathway in the cat. III. Cerebellar input to corticofugal neurons destined for different subcortical nuclei in areas 4 and 6. *Neurosci Res* 3: 321–344, 1986.

Gerstner W, van Hemmen JL, and Cowan JD. What matters in neuronal locking? *Neural Comput* 8: 1653–1676, 1996.

Gibson JR, Beierlein M, and Connors BW. Two networks of electrically coupled inhibitory neurons in neocortex. *Nature* 402: 75–79, 1999.

Gray CM, Engel AK, Konig P, and Singer W. Stimulus-dependent neuronal oscillations in cat visual-cortex - receptive-field properties and feature dependence. *Eur J Neurosci* 2: 607–619, 1990.

Gray CM, Konig P, Engel AK, and Singer W. Oscillatory responses in cat visual-cortex exhibit inter-columnar synchronization which reflects global stimulus properties. *Nature* 338: 334–337, 1989.

Halliday DM. Weak, stochastic temporal correlation of large scale synaptic input is a major determinant of neuronal bandwidth. *Neural Comput* 12: 693–707, 2000.

Hansel D, Mato G, and Meunier C. Synchrony in excitatory neural networks. *Neural Comput* 7: 307–337, 1995.

Hartmann MJ and Bower JM. Oscillatory activity in the cerebellar hemispheres of unrestrained rats. *J Neurophysiol* 80: 1598–1604, 1998.

Hentschke H, Schwarz C, and Antkowiak B. Neocortex is the major target of sedative concentrations of volatile anaesthetics: strong depression of firing rates and increase of GABAA receptor-mediated inhibition. *Eur J Neurosci* 21: 93–102, 2005.

Holdefer RN, Miller LE, Chen LL, and Houk JC. Functional connectivity between cerebellum and primary motor cortex in the awake monkey. *J Neurophysiol* 84: 585–590, 2000.

Hoover JE and Strick PL. The organization of cerebellar and basal ganglia outputs to primary motor cortex as revealed by retrograde transneuronal transport of herpes simplex virus type 1. *J Neurosci* 19: 1446–1463, 1999.

Hubbard JI, Llinas R, and Quastel DMJ. *Electrophysiological Analysis of Synaptic Transmission.* London: Edward Arnold, 1969.

Huber J, Grottel K, and Celichowski J. Dual projections of the ventromedial lamina VI and the medial lamina VII neurones in the second sacral spinal cord segment to the thalamus and the cerebellum in the cat. *Neurosci Res* 21: 51–57, 1994.

Hummelsheim H, Wiesendanger R, Wiesendanger M, and Bianchetti M. The projection of low-threshold muscle afferents of the forelimb to the main and external cuneate nuclei of the monkey. *Neuroscience* 16: 979–987, 1985.

Ito M. *Control System Model of the Cerebellum. The Cerebellum and Neuronal Control.* New York: Raven Press, 1984.

Jackson A, Gee VJ, Baker SN, and Lemon RN. Synchrony between neurons with similar muscle fields in monkey motor cortex. *Neuron* 38: 115–125, 2003.

Kawamura K and Chiba M. Cortical neurons projecting to the pontine nuclei in the cat. An experimental study with the horseradish peroxidase technique. *Exp Brain Res* 35: 269–285, 1979.

Keating JG and Thach WT. No clock signal in the discharge of neurons in the deep cerebellar nuclei. *J Neurophysiol* 77: 2232–2234, 1997.

Kelly RM and Strick PL. Cerebellar loops with motor cortex and prefrontal cortex of a nonhuman primate. *J Neurosci* 23: 8432–8444, 2003.

Kilner JM, Baker SN, Salenius S, Hari R, and Lemon RN. Human cortical muscle coherence is directly related to specific motor parameters. *J Neurosci* 20: 8838–8845, 2000.

Kilner JM, Baker SN, Salenius S, Jousmäki V, Hari R, and Lemon RN. Task-dependent modulation of 20–30 Hz coherence between rectified EMGs from human hand and forearm muscles. *J Physiol* 516: 559–570, 1999.

Konig P and Engel AK. Correlated firing in sensory-motor systems. *Curr Opin Neurobiol* 5: 511–519, 1995.

Lebedev MA and Wise SP. Oscillations in the premotor cortex: single-unit activity from awake, behaving monkeys. *Exp Brain Res* 130: 195–215, 2000.

Lee D. Behavioral context and coherent oscillations in the supplementary motor area. *J Neurosci* 24: 4453–4459, 2004.

Lemon RN. Methods for neuronal recording in conscious animals. In: *IBRO Handbook Series: Methods in Neurosciences.* London: Wiley, 1984.

Li CL and Tew JM Jr. The effect of cerebellar stimulation on neuronal activity in the motor cortex. *Exp Neurol* 14: 317–327, 1966.

MacKay WA. Synchronised neuronal oscillations and their role in motor processes. *Trends Cogn Sci* 1: 176–182, 1997.

MacKay WA and Mendonca AJ. Field potential oscillatory bursts in parietal cortex before and during reach. *Brain Res* 704: 167–174, 1995.

Marsden JF, Ashby P, Limousin-Dowsey P, Rothwell JC, and Brown P. Coherence between cerebellar thalamus, cortex and muscle in man: cerebellar thalamus interactions. *Brain* 123: 1459–1470, 2000.

Massopust LC, Hauge DH, Ferneding JC, Doubek WG, and Taylor JJ. Projection systems and terminal localization of dorsal column afferents: an autoradiographic and horseradish peroxidase study in the rat. *J Comp Neurol* 237: 533–544, 1985.

Mihailoff GA. Intra- and interhemispheric collateral branching in the rat pontocerebellar system, a fluorescence double-label study. *Neuroscience* 10: 141–160, 1983.

Miller LE and Houk JC. Motor co-ordinates in primate red nucleus: preferential relation to muscle activation versus kinematic variables. *J Physiol* 488: 533–548, 1995.

Mock M, Schwarz C, and Thier P. Electrophysiological properties of rat pontine nuclei neurons in vitro II. Postsynaptic potentials. *J Neurophysiol* 78: 3338–3350, 1997.

Mountcastle VB, Reitboeck HJ, Poggio GF, and Steinmetz MA. Adaptation of the Reitboeck method of multiple microelectrode recording to the neocortex of the waking monkey. *J Neurosci Methods* 36: 77–84, 1991.

Murthy VN and Fetz EE. Coherent 25- to 35-Hz oscillations in the sensorimotor cortex of awake behaving monkeys. *Proc Natl Acad Sci USA* 89: 5670–5674, 1992.

Murthy VN and Fetz EE. Oscillatory activity in sensorimotor cortex of awake monkeys: synchronization of local field potentials and relation to behavior. *J Neurophysiol* 76: 3949–3967, 1996a.

Murthy VN and Fetz EE. Synchronization of neurons during local field potential oscillations in sensorimotor cortex of awake monkeys. *J Neurophysiol* 76: 3968–3982, 1996b.

Nicolelis MAL, Baccala LA, Lin RCS, and Chapin JK. Sensorimotor encoding by synchronous neural ensemble activity at multiple levels of the somatosensory system. *Science* 268: 1353–1358, 1995.

Niimi K, Fujiwara N, Takimoto T, and Matsugi S. The course and termination of the ascending fibers of the brachium conjunctivum in the cat as studied by the Nauta method. *Tokushima J Exp Med* 8: 269–284, 1962.

Noda H, Murakami S, Yamada J, Tamada J, Tamaki Y, and Aso T. Saccadic eye movements evoked by microstimulation of the fastigial nucleus of macaque monkeys. *J Neurophysiol* 60: 1036–1052, 1988.

Noda T and Yamamoto T. Response properties and morphological identification of neurons in the cat motor cortex. *Brain Res* 306: 197–206, 1984.

O'Connor SM, Berg RW, and Kleinfeld D. Coherent electrical activity between vibrissa sensory areas of cerebellum and neocortex is enhanced during free whisking. *J Neurophysiol* 87: 2137–2148, 2002.

Oscarsson O. Functional organisation of spinocerebellar paths. In: *Handbook of Sensory Physiology,* edited by Autrum H, Jung R, Loewenstein W, MacKay D, and Teuber H. New York: Springer-Verlag, 1973, p. 340–373.

Palkovits M, Mezey E, Hamori J, and Szentagothai J. Quantitative histological analysis of the cerebellar nuclei in the cat. I. Numerical data on cells and on synapses. *Exp Brain Res* 28: 189–209, 1977.

Pauluis Q, Baker SN, and Olivier E. Emergent oscillations in a realistic network: the role of inhibition and the effect of the spatiotemporal distribution of the input. *J Comp Neurosci* 6: 289–310, 1999.

Pellerin JP and Lamarre Y. Local field potential oscillations in primate cerebellar cortex during voluntary movement. *J Neurophysiol* 78: 3502–3507, 1997.

Perkel DH, Gerstein GL, and Moore GP. Neuronal spike trains and stochastic point processes. I. The single spike train. *Biophys J* 7: 391–418, 1967.

Pfurtscheller G and Neuper C. Simultaneous EEG 10 Hz desynchronization and 40 Hz synchronization during finger movements. *Neuroreport* 3: 1057–1060, 1992.

Pfurtscheller G, Neuper C, and Kalcher J. 40-Hz oscillations during motor behavior in man. *Neurosci Lett* 164: 179–182, 1993.

Riddle CN and Baker SN. Manipulation of peripheral neural feedback loops alters human corticomuscular coherence. *J Physiol* 566: 625–639, 2005.

Roelfsema PR, Engle AK, Konig P, and Singer W. Visuomotor integration is associated with zero time-lag synchronization among cortical areas. *Nature* 385: 157–161, 1997.

Rosenberg JR, Amjad AM, Breeze P, Brillinger DR, and Halliday DM. The Fourier approach to the identification of functional coupling between neuronal spike trains. *Prog Biophys Mol Biol* 53: 1–31, 1989.

Rosina A, Provini L, Bentivoglio M, and Kuypers HG. Ponto-neocerebellar axonal branching as revealed by double fluorescent retrograde labeling technique. *Brain Res* 195: 461–466, 1980.

Salenius S, Schnitzler A, Salmelin R, Jousmaki V, and Hari R. Modulation of human cortical rolandic rhythms during natural sensorimotor tasks. *Neuroimage* 5: 221–228, 1997.

Sanes JN and Donoghue JP. Oscillations in local-field potentials of the primate motor cortex during voluntary movement. *Proc Natl Acad Sci USA* 90: 4470–4474, 1993.

Shadlen MN and Newsome WT. The variable discharge of cortical neurons: implications for connectivity, computation, and information coding. *J Neurosci* 18: 3870–3896, 1998.

Shinoda Y, Kano M, and Futami T. Synaptic organization of the cerebellothalamo-cerebral pathway in the cat. I. Projection of individual cerebellar nuclei to single pyramidal tract neurons in areas 4 and 6. *Neurosci Res* 2: 133–156, 1985.

Shinoda Y, Sugiuchi Y, and Futami T. Excitatory inputs to cerebellar dentate nucleus neurons from the cerebral cortex in the cat. *Exp Brain Res* 67: 299–315, 1987.

Singer W. Time as coding space? *Curr Opin Neurobiol* 9: 189–194, 1999.

Somana R and Walberg F. A re-examination of the cerebellar projections from the gracile, main and external cuneate nuclei in the cat. *Brain Res* 186: 33–42, 1980.

Stopfer M, Bhagavan S, Smith BH, and Laurent G. Impaired odour discrimination on desynchronization of odour-encoding neural assemblies. *Nature* 390: 70–74, 1997.

Strick PL and Sterling P. Synaptic termination of afferents from the ventrolateral nucleus of the thalamus in the cat motor cortex. A light and electron microscopy study. *J Comp Neurol* 153: 77–106, 1974.

Sturm AK and Konig P. Mechanisms to synchronize neuronal activity. *Biol Cyber* 84: 153–172, 2001.

Swadlow HA, Rosene DL, and Waxman SG. Characteristics of interhemispheric impulse conduction between prelunate gyri of the rhesus monkey. *Exp Brain Res* 33: 455–467, 1978.

Tarnecki R and Zurawska I. Functional relations between neighboring neurons of nucleus interpositus of the cat cerebellum. *Acta Physiol Pol* 40: 456–472, 1989.

Timofeev I and Steriade M. Fast (mainly 30–100 Hz) oscillations in the catcerebellothalamic pathway and their synchronization with cortical potentials *J Physiol* 504: 153–168, 1997.

Ugolini G and Kuypers HG. Collaterals of corticospinal and pyramidal fibres to thepontine grey demonstrated by a new application of the fluorescent fibre labelling technique. *Brain Res* 365: 211–227, 1986.

Van Vreeswijk C, Abbott LF, and Ermentrout GB. When inhibition not excitationsynchronizes neural firing. *J Comp Neurosci* 1: 313–321, 1994.

Welsh JP, Lang EJ, Suglhara I, and Llinas R. Dynamic organization of motor controlwithin the olivocerebellar system. *Nature* 374: 453–457, 1995.

Welsh JP and Llinas R. Some organizing principles for the control of movementbased on olivocerebellar physiology. *Prog Brain Res* 114: 449–461, 1997.

Wetmore DZ and Baker SN. Post-spike distance-to-threshold trajectories of neuronesin monkey motor cortex. *J Physiol* 555: 831–850, 2004.